



# Structural, biophysical, and biochemical insights into C–S bond cleavage by dimethylsulfone monooxygenase

Reyaz Gonzalez<sup>a</sup>, Jess Soule<sup>a,1</sup> , Ngan Phan<sup>b,2</sup> , Denyce K. Wicht<sup>b</sup>, and Daniel P. Dowling<sup>a,3</sup>

Affiliations are included on p. 11.

Edited by Tadhg P. Begley, Texas A&M University, College Station, TX; received January 27, 2024; accepted September 23, 2024 by Editorial Board Member Stephen J. Benkovic

Sulfur is an essential element for life. Bacteria can obtain sulfur from inorganic sulfate; but in the sulfur starvation–induced response, *Pseudomonads* employ two-component flavin-dependent monooxygenases (TC-FMOs) from the *msu* and *sfn* operons to assimilate sulfur from environmental compounds including alkanesulfonates and dialkylsulfones. Here, we report binding studies of oxidized FMN to enzymes involved within the *P. fluorescens* enzymatic pathway responsible for converting dimethylsulfone (DMSO<sub>2</sub>) to sulfite. In this catabolic pathway, SfnG serves as the initial TC-FMO for sulfur assimilation, which is investigated in detail by solving the 2.6-Å resolution crystal structure of unliganded SfnG and the 1.75-Å resolution crystal structure of the SfnG ternary complex containing FMN and DMSO<sub>2</sub>. We find that SfnG adopts a  $(\beta/\alpha)_8$  barrel fold with a distinct quaternary configuration from other tetrameric class C TC-FMOs. To probe the unexpected tetramer arrangement, structural heterogeneity is assessed by chromatography and light scattering to confirm ligand binding correlates with a tetramer. Binding of FMN and DMSO<sub>2</sub> accompanies ordering of the active site, with DMSO<sub>2</sub> bound on the *si*-face of the flavin. A previously unobserved protein backbone conformation is found within the oxygen-binding site on the *re*-face of the flavin. Functional assays and the positioning of ligands with respect to the oxygen-binding site are consistent with use of an N5-(hydro)peroxyflavin pathway. Biochemical endpoint assays and docking studies reveal SfnG breaks the C–S bond of a range of dialkylsulfones.

flavin | N5-(hydro)peroxyflavin | TIM barrel | FMN | dialkylsulfone

Bacterial flavoprotein monooxygenases (FPMOs) are an important source of chemically useful transformations (1–3). FPMO chemistries usually occur via formation of the C4a-(hydro)peroxyflavin pathway, but more recently a subset of monooxygenases are proposed to use an N5-(hydro)peroxyflavin pathway (Fig. 1A) (4–10). Among these redox proteins are two-component flavin-dependent monooxygenases (TC-FMOs), which rely on a separate NAD(P)H-dependent flavin reductase to provide reduced flavin mononucleotide (FMNH<sup>−</sup>) or flavin adenine dinucleotide (FADH<sup>−</sup>) (Fig. 1A) (1). FMNH<sup>−</sup> is a cosubstrate that must be transferred between the reductase and monooxygenase during the reaction cycle. The separation of reductase and monooxygenase activities makes TC-FMOs particularly attractive for bioengineering of the monooxygenase without altering the reductase. However, before TC-FMOs can be rationally bioengineered, we must understand flavin transfer, substrate binding, catalysis, and oxygen sensing. To explore features of TC-FMO function, we study the bacterial sulfur assimilation pathway from dimethylsulfone (DMSO<sub>2</sub>) (Fig. 1B), an organosulfur compound derived from oxidation of environmental dimethylsulfide (DMS) (11–13) that serves as a sulfur or carbon source for several species of bacteria (14). Additionally, sulfur assimilation pathways are of interest as potential targets against pathogenic fungi (15). DMSO<sub>2</sub> is linked to the intestinal microbiome through degradation of methionine, resulting in DMS (16). DMS can undergo host bioconversion to DMSO<sub>2</sub> (16), making DMSO<sub>2</sub> a possible source of sulfur for pathogenic bacteria. DMSO<sub>2</sub> also is bacteriostatic at high concentrations for multiple drug-resistant strains of *Escherichia coli* and *Salmonella enterica* (17).

Sulfur is an essential element for life (18) and is typically acquired by soil-dwelling bacteria as sulfate, which is processed downstream to sulfide and used in biosynthetic and signaling pathways. In sulfate-limited environments, bacteria acquire sulfur from organosulfur compounds (11, 19, 20), a process which mandates overcoming the chemical challenge of cleaving stable C–S bonds (21–23). Bacteria utilize oxygenases to catabolize organosulfur products of the global sulfur cycle such as DMSO<sub>2</sub>, alkanesulfonates, dibenzothiophene (DBT), and taurine (21, 22, 24, 25). For dialkylsulfones and alkanesulfonates, the monooxygenases incorporate one oxygen atom derived from molecular oxygen at the C1 substrate

## Significance

Here, we investigate structural features that facilitate C–S bond cleavage of dimethylsulfone (DMSO<sub>2</sub>) by the flavoprotein monooxygenase SfnG from *Pseudomonas fluorescens*. DMSO<sub>2</sub> can serve as an alternative sulfur source for bacterial survival during sulfur starvation. The structures of SfnG provide insights into two-component flavin-dependent monooxygenases that adopt a  $(\beta/\alpha)_8$  barrel fold and demonstrate a distinct tetramer configuration within this family. Our results are consistent with C–S bond cleavage proceeding through a flavin-N5 oxygen adduct and reveal snapshots of changes within the oxygen-binding site. Activity and flavin binding studies provide active site details that may be exploited for catalytic engineering or inhibition of related systems.

Author contributions: R.G., J.S., D.K.W., and D.P.D. designed research; R.G., J.S., N.P., and D.K.W. performed research; R.G., J.S., N.P., D.K.W., and D.P.D. analyzed data; and R.G., J.S., D.K.W., and D.P.D. wrote the paper.

The authors declare no competing interest.

This article is a PNAS Direct Submission. T.P.B. is a guest editor invited by the Editorial Board.

Copyright © 2024 the Author(s). Published by PNAS. This article is distributed under Creative Commons Attribution-NonCommercial-NoDerivatives License 4.0 (CC BY-NC-ND).

<sup>1</sup>Present address: Department of Chemistry and Biochemistry, University of California, Los Angeles, CA 90095.

<sup>2</sup>Present address: Department of Molecular and Cell Biology, University of California, Berkeley, CA 94720.

<sup>3</sup>To whom correspondence may be addressed. Email: daniel.dowling@umb.edu.

This article contains supporting information online at <https://www.pnas.org/lookup/suppl/doi:10.1073/pnas.2401858121/-DCSupplemental>.

Published November 12, 2024.

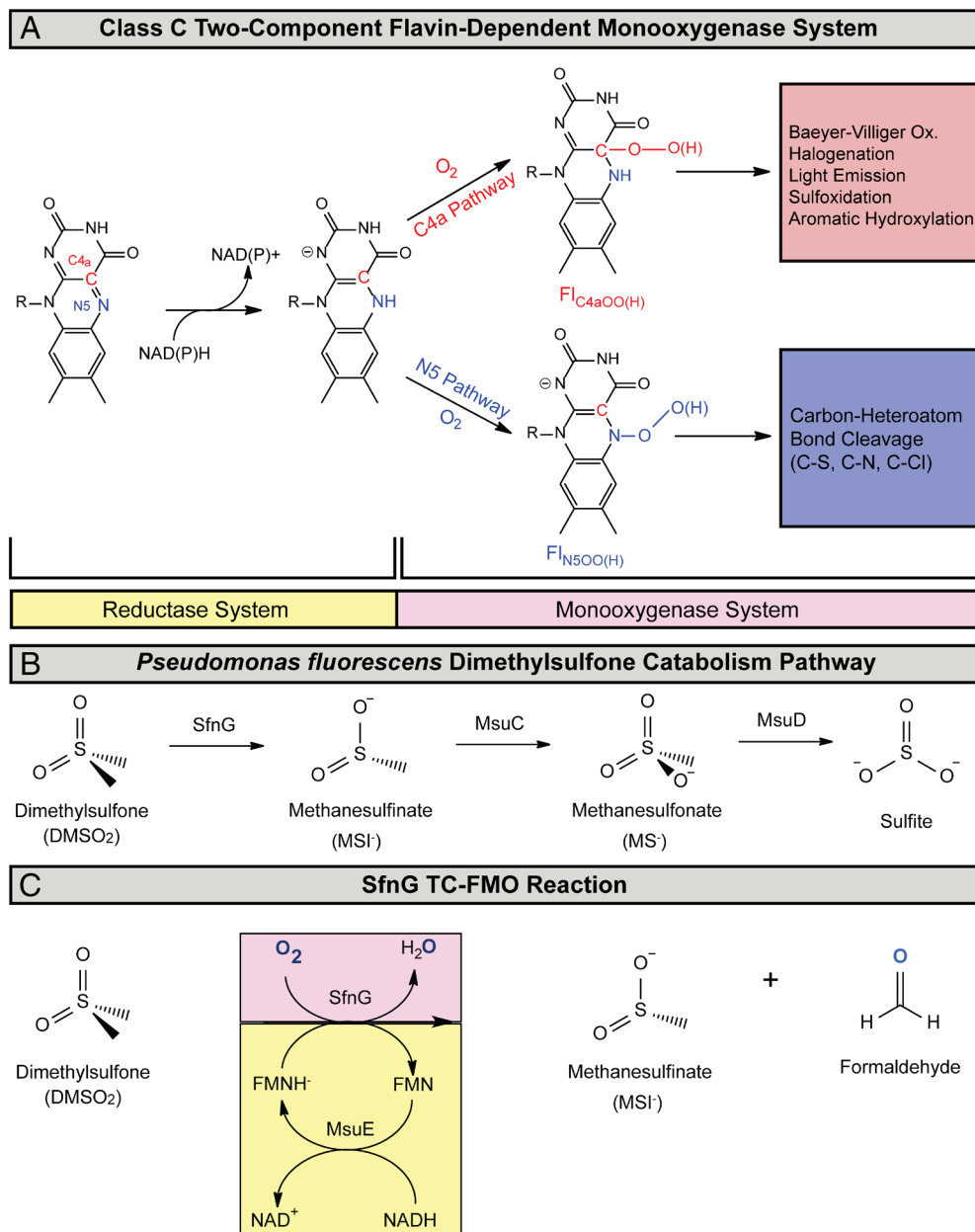


**Fig. 1.** Bacterial sulfur assimilation of  $\text{DMSO}_2$  in *Pseudomonads* under sulfur starvation conditions requires TC-FMOs SfnG, MsuC, and MsuD. (A) Schematic representation of flavin's bifurcation into two prominent pathways, the N5 and C4a pathways, highlighting their respective unique chemistries and the intricate versatility of flavin in governing diverse catalytic reactions within biological systems (1). (B) The pathway of  $\text{DMSO}_2$  catabolism to sulfite consists of three TC-FMOs, each of which requires an FMN reductase, such as MsuE, to generate reduced FMN for activity. (C) The overall TC-FMO reaction scheme for SfnG is displayed with the reductase MsuE.

position to generate an aldehyde, and the second oxygen atom is eventually released as water (Fig. 1C) (21, 23, 26). The pathway for oxidative conversion of  $\text{DMSO}_2$  to sulfite was proposed in the genetically tractable *P. fluorescens* (6, 24). The monooxygenase is encoded in an isolated gene *sfnG* and the FMN reductase MsuE from the methanesulfonate utilization (*msu*) operon is used to reconstitute monooxygenase activity (24). The sulfur assimilation pathway from  $\text{DMSO}_2$  (Fig. 1B) involves sequential conversion of  $\text{DMSO}_2$  ( $S + 2$ ) to methanesulfinate ( $\text{MSI}^-$ ,  $S + 2$ ) via C–S bond cleavage by the monooxygenase SfnG (24), and oxidation of  $\text{MSI}^-$  to methanesulfonate ( $\text{MS}^-$ ,  $S + 4$ ) by methanesulfinate monooxygenase MsuC (27). In the final step of this pathway, alkanesulfonate monooxygenase MsuD converts  $\text{MS}^-$  to sulfite (6).

Despite the strong interest in FMO systems as biocatalysts (1), there is a limited number of high-resolution structures for TC-FMOs, and even fewer structures with bound flavin and substrate.

Considering class C TC-FMOs require both substrates for ordering of the active site (28), additional high-resolution structures are needed. Here, we report crystal structures of SfnG both with and without oxidized flavin mononucleotide (FMN) and  $\text{DMSO}_2$ . The 1.75-Å resolution crystal structure of SfnG characterizes ligand placement in the active site for reaction chemistry to proceed. To better understand specificity and mechanism, we interrogate SfnG activity against mixed methylthiolsulfone and diethylsulfone through an NMR spectroscopy endpoint assay and LC–MS trapping of an abortive flavin N5 oxide species. These results, coupled with functional mutations, confirm SfnG utilizes a putative N5-(hydro)peroxyflavin species to ultimately convert  $\text{DMSO}_2$  to methanesulfinate and define active site features that provide insight into SfnG substrate specificity. To characterize flavin transfer within enzymes of the dialkylsulfone utilization pathway of *P. fluorescens*, we measured the binding affinities for FMN within the pathway.

The SfnG structures reveal a protein conformation within the oxygen-binding site that may interact with water when bound, a conformation previously unseen in class C TC-FMOs. The structure and biophysical experiments detail an unexpected tetramer formation that is distinct from other TC-FMOs, providing avenues for future bioengineering and inhibitor development to target bacterial sulfur assimilation pathways.

## Results

**Investigations of FMN Binding within the *P. fluorescens* DMSO<sub>2</sub> Utilization Pathway.** FMN and FMNH<sup>-</sup> are respective substrates for the reductase and monooxygenase enzymes, therefore we studied the affinities for FMN binding to the four sulfur assimilation enzymes via spectrofluorometric titration and surface plasmon resonance (SPR) for SfnG and MsuE (Fig. 2). The equilibrium titration of MsuE with FMN over the concentration range 0.033 μM to 260 μM results in a  $K_D$  value of  $0.54 \pm 0.06$  μM, consistent with 1:1 tight binding of FMN to MsuE. The equilibrium titrations of SfnG, MsuC, and MsuD with FMN were performed over concentrations ranging from 0.2 μM to 300 μM (for SfnG) and 0.2 μM to 400 μM (for MsuC and MsuD) (*SI Appendix, Supporting Methods*). The  $K_D$  values are an order of magnitude higher than observed for MsuE, consistent with weaker binding of FMN by the monooxygenases. Binding of FMN to SfnG and MsuE was also interrogated by SPR using protein immobilized on a nitrilotriacetic acid (NTA) sensor chip (Fig. 2B) (*SI Appendix, Supporting Methods*). SPR with hexahistidine-tagged proteins may demonstrate issues with immobilization stability due to the relatively weak interaction of the hexahistidine tag with the NTA sensor chip surface (29). This instability can influence the choice of kinetic analysis employed. The measurements of SfnG and MsuE binding parameters required a capture method coupled with multicycle kinetic analysis to minimize baseline drift and achieve acceptable fit statistics. Injections of FMN showed SPR injection spikes at higher FMN concentrations, indicative of FMN solubility issues (*SI Appendix, Fig. S1*). Standard supplementation of running buffer with 1% (v/v) DMSO removed injection spikes (Fig. 2B). Intriguingly, the  $k_{on}$  for FMN is observed to be in a similar magnitude range for MsuE and the monooxygenase SfnG, whereas the  $k_{off}$  for FMN is about twofold smaller for MsuE. We note that without 1% (v/v) DMSO present, the  $k_{on}$  is ~2-fold lower for SfnG relative to MsuE, and the SPR  $K_D$  values are closer to the  $K_D$  determined by spectrofluorometric titration. To verify whether DMSO has a similar effect on MsuE, SPR experiments were conducted using the same running buffer supplemented with 1% (v/v) DMSO. The  $K_D$  of MsuE increased significantly; consequently, DMSO was not used for further MsuE SPR experiments. During the dissociation phase, SfnG and MsuE show a delay in flavin release that is most noticeable at FMN concentrations at and above 10 μM. The  $K_D$  trends are consistent by both SPR and spectrophotometric titration, with submicromolar FMN affinities for the reductase MsuE and decreased relative affinity for the monooxygenase SfnG. Considering that the monooxygenase SfnG is predicted to demonstrate an ordered binding mechanism based on homologous TC-FMO systems (30, 31), the off rate for FMN was further explored by including 0.1 mM DMSO<sub>2</sub> in the running buffer. The addition of DMSO<sub>2</sub> decreased the  $k_{off}$  rate constant from  $0.42 \text{ s}^{-1}$  to  $8.36 \times 10^{-3} \text{ s}^{-1}$  (*SI Appendix, Fig. S2*), presumably due to binding of DMSO<sub>2</sub> after FMN binding occurs. The observed 2.7-fold decrease in  $K_D$  by SPR for SfnG when 1% (v/v) DMSO is in the running buffer may similarly be a result of weak binding of DMSO, although SfnG is not active against DMSO (32). After determining the monooxygenase binding of FMN, we set

forth to obtain a structure with DMSO<sub>2</sub> bound in the presence of FMN to prevent enzyme turnover. Although FMN is a product of the monooxygenase, we expected FMN to bind similarly to the FMNH<sup>-</sup> substrate and enable DMSO<sub>2</sub> binding.

**The 2.6-Å and 1.75-Å Resolution Crystal Structures of SfnG.** SfnG from *P. fluorescens* was crystallized in both the ternary (SfnG-FMN-DMSO<sub>2</sub>) and unliganded states. The 2.6-Å resolution crystal structure of unliganded SfnG was solved by molecular replacement using *Bacillus cereus* luciferase-like monooxygenase (PDB ID: 3RAO) (33) as a search model. SfnG crystallized in space group *P*1 with eight protein chains per asymmetric unit (*SI Appendix, Table S2*). The unliganded SfnG structure was used as a molecular replacement search model for the 1.75-Å resolution ternary SfnG structure, which was obtained by cocrystallization in the presence of excess ligands. The ternary complex crystallized in space group *C*222<sub>1</sub>, with eight protein chains per asymmetric unit (*SI Appendix, Table S2*). The structure of SfnG adopts the  $(\beta/\alpha)_8$  TIM-barrel fold (34), consistent with SfnG being a group C flavin-dependent monooxygenase (Fig. 3*A*) (1). The TIM barrel fold is accompanied by three insertion regions (IR) to the  $(\beta/\alpha)_8$  core and one extension region (ER) after the core: IR-1 is a lone  $\alpha$ -helix ( $\alpha$ 4, F122–I129), IR-2 includes a  $\beta$ -hairpin ( $\beta$ 5,  $\beta$ 6, F159–Y171), IR-3 consists of a bundle of three  $\alpha$ -helices (T244–N303), and ER-1 (Q342–A361) consists of an extension of the C-terminal  $\alpha$ -helix of the protein core, generating a kinked helix (*SI Appendix, Fig. S3*). Details for the final model are included within *SI Appendix, Supporting Methods*.

The SfnG protomer arranges as a dimer of dimers (Fig. 3*A* and *B*), burying approximately 1,750 Å<sup>2</sup> at each dimer interface and approximately 1,500 Å<sup>2</sup> at the tetramer interface, determined by the PISA server (35). The dimer interface consists of helices  $\alpha$ 2 and  $\alpha$ 3 of the  $(\beta/\alpha)_8$  core and IR-1 and IR-2, and the tetramer interface includes helices  $\alpha$ 4 of IR-1 and  $\alpha$ 5 of the  $(\beta/\alpha)_8$  core and IR-2. Interactions at the dimer interface are made up of hydrophobic packing and polar interactions, whereas the tetramer interface is largely stabilized by electrostatic and polar interactions (Fig. 3 *C* and *D*). Additionally, an internal solvent cavity is observed within the tetramer (*SI Appendix, Fig. S4 A and B*). Initial SEC purification of SfnG resulted in the elution of two species best matching a dimer and tetramer, creating ambiguity regarding the functional quaternary structure (*SI Appendix, Fig. S4C*). We hypothesized that high salt could disrupt the tetramer assembly; therefore, SfnG was incubated in high (500 mM NaCl) and low (100 mM NaCl) salt conditions and analyzed by analytical size exclusion chromatography (aSEC) (*SI Appendix, Fig. S5*). An elution peak assigned to the tetramer was observed in low salt at 11.2 mL and a broad elution peak assigned to the dimer in high salt at 12.3 mL, suggesting salt indeed disrupts the tetramer. Samples were further analyzed by SEC coupled with multiangle light scattering (SEC-MALS) and dynamic light scattering (DLS) to determine solution molecular weight, particle size, and alterations in percent polydispersity (% PD) as a function of salt concentration (Fig. 3 *E* and *F*). Incubation of 1 mg/mL SfnG with 500 mM NaCl led to an increased population of a smaller species ~3.8 nm in radius, decreasing the overall hydrodynamic radius and doubling the % PD by DLS. These same conditions resulted in a broad elution peak at 13.1 min in SEC-MALS corresponding to 80 kDa and a minor aggregate peak at 7.5 min. Last, we wished to probe the effects of FMN, DMSO<sub>2</sub>, and FMN+DMSO<sub>2</sub> binding on SfnG in low and high salt (Fig. 3 *E* and *F* and *SI Appendix, Fig. S6*). We observed no significant change by DLS with ligand binding in low salt conditions. In high salt conditions, SEC-MALS revealed the introduction of FMN

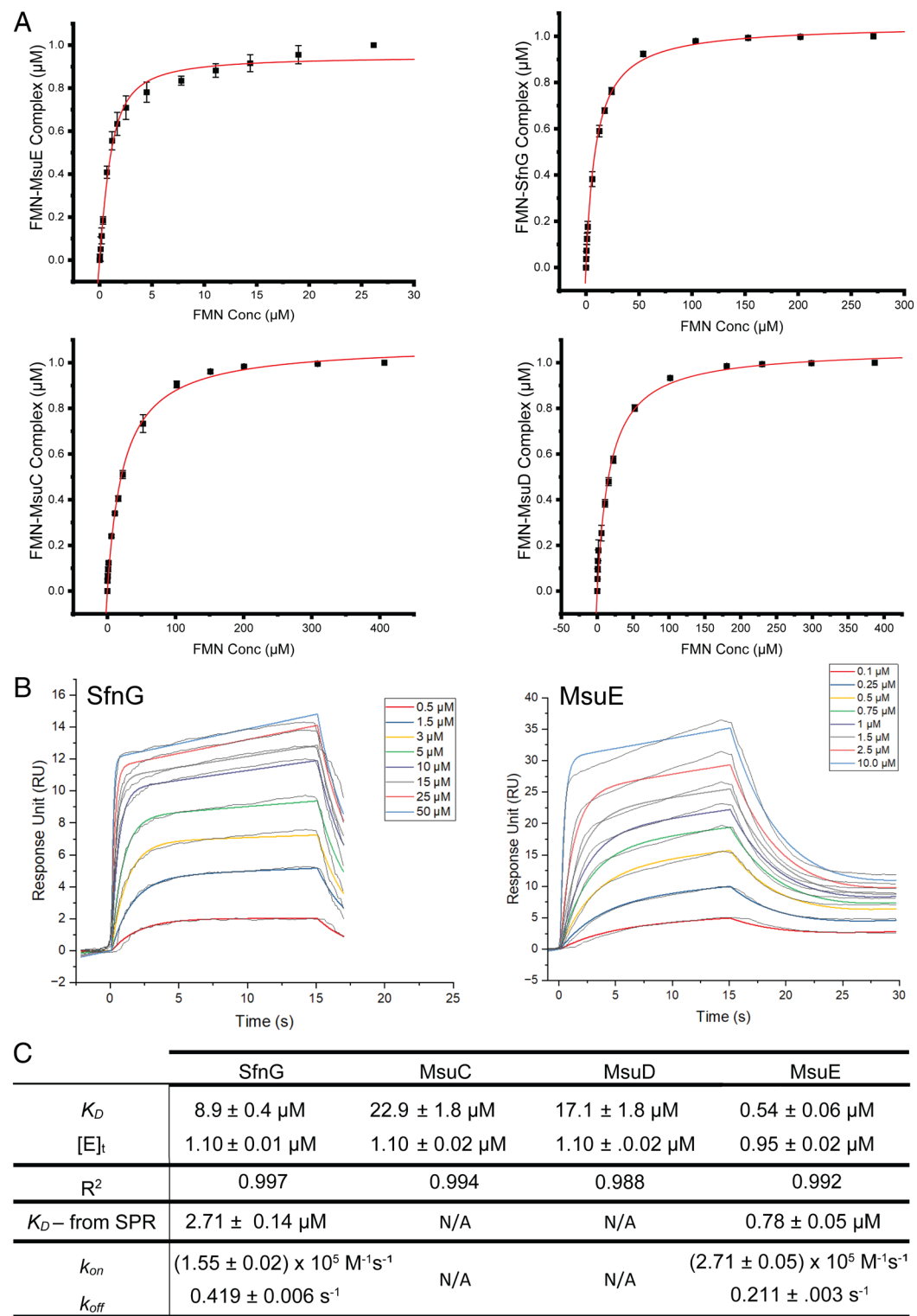


**Fig. 2.** FMN binding assays of the *P. fluorescens* DMSO<sub>2</sub> utilization pathway reveal tighter binding to the reductase compared to the monooxygenases. (A) Equilibrium binding of FMN by MsuE, SfnG, MsuC, and MsuD was measured by intrinsic fluorescence. (B) The kinetics of FMN binding to TC-FMO SfnG and flavin reductase MsuE were monitored using SPR spectroscopy with multicycle kinetics. Raw data are shown in black overlaid with labeled kinetic fits. (C) The binding parameters for SfnG, MsuC, MsuD, and MsuE from fluorescence titration are shown, with equilibrium binding constant ( $K_D$ ), total enzyme ([E]<sub>t</sub>), and R<sup>2</sup> values from the corresponding fit for each enzyme, ±SD from three assay replicates. The resulting  $k_{on}$  and  $k_{off}$  rate constants and  $K_D$  from SPR experiments are included for MsuE and SfnG, ±SE values.

and DMSO<sub>2</sub> at 5× molar excess shifted retention time to 11.3 min with a molecular weight of 160 kDa by MALS and two minor peaks at 7.5 min and 10 min, corresponding to higher molecular weight aggregates. The presence of FMN or FMN+DMSO<sub>2</sub> similarly decreased the population of the 3.8 nm radius species assigned to the dimer, restoring a lower % PD and a radius of the

tetramer by DLS, whereas DMSO<sub>2</sub> alone had no effect. Therefore, the tetrameric quaternary structure of SfnG is stabilized by FMN and DMSO<sub>2</sub> binding, and DMSO<sub>2</sub> binding is dependent on the presence of FMN.

SfnG is most similar in structure to other class C flavin-dependent monooxygenases, despite sharing less than 34% sequence identity.

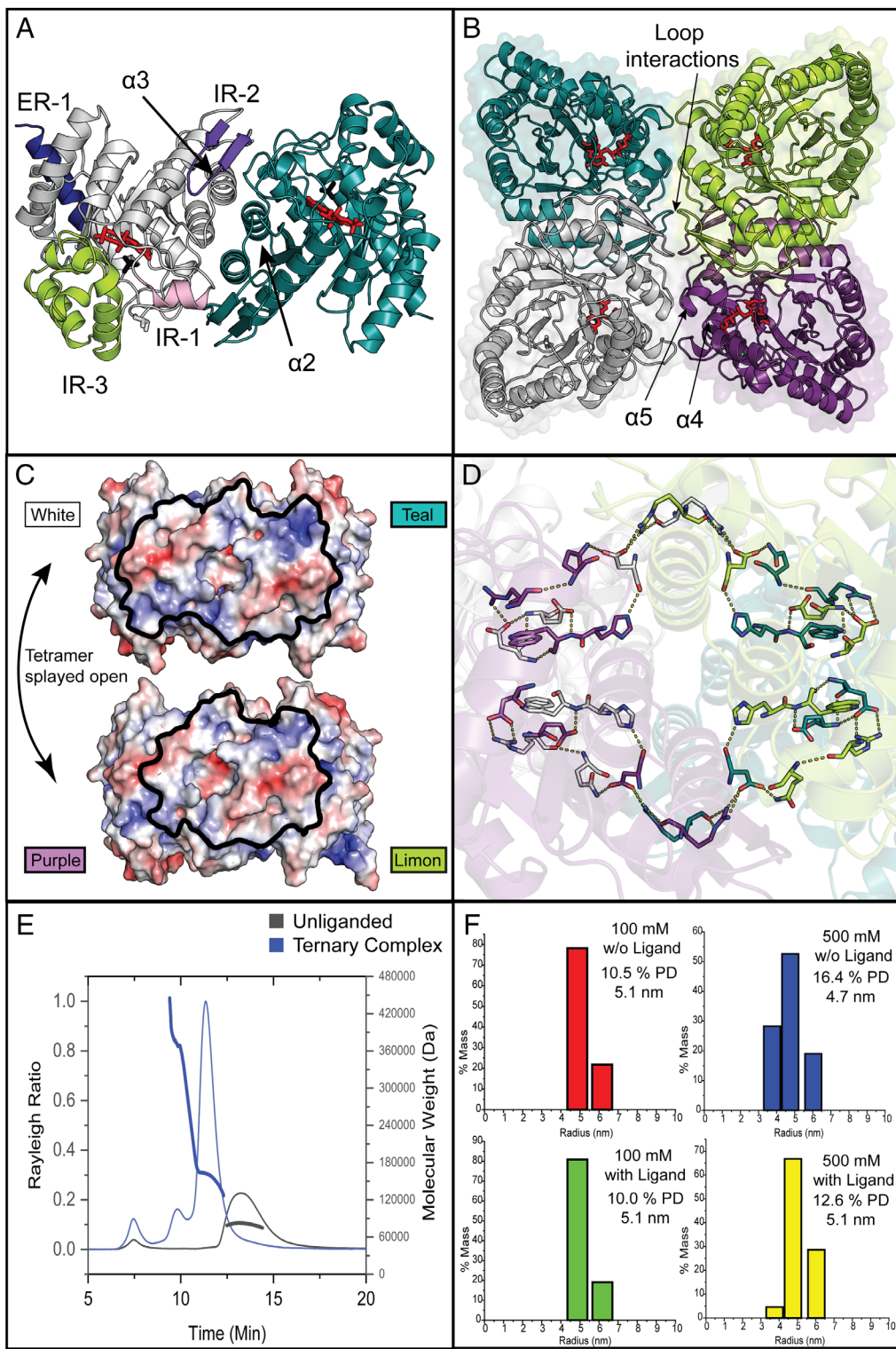


**Fig. 3.** The overall crystal structure of *P. fluorescens* SfnG reveals a tetramer interface consisting of a hydrogen-bonding network and salt bridges. (A) A dimer of SfnG is shown in cartoon representation with FMN and DMSO<sub>2</sub> in red and black sticks, respectively. SfnG adopts a  $\beta/\alpha$ <sub>8</sub> TIM barrel fold (white), with insertion and extension regions colored as follows: IR-1, light pink; IR-2, purple; IR-3, limon; and ER-1, blue. The C<sub>2</sub> symmetry-related molecule is colored teal. (B) The butterfly-arranged tetramer of SfnG is shown, with individual protomers colored teal, gray, limon, and purple. (C) The APBS surface electrostatic potential of each SfnG dimer is displayed as a gradient from red (negative) to blue (positive), mapped to  $\pm 5 k_B T_c^{-1}$ , with the tetramer splayed open and the tetramer interface highlighted with a black outline. Individual protomers are labeled with the color scheme shown in B. (D) The hydrogen-bonding network and salt bridges at the tetramer interface are shown, with protomers colored as in panel B. Atoms are colored as follows: oxygen, red; nitrogen, blue; and carbons, matched to protomers as in B. (E) SEC-MALS traces and molecular weight distribution are shown of SfnG in high salt buffer with and without FMN and DMSO<sub>2</sub>. (F) The hydrodynamic radius of SfnG was determined by DLS under varying NaCl concentrations, with and without FMN and DMSO<sub>2</sub>.

The closest reported structures to SfnG are *B. cereus* luciferase-like monooxygenase (seq. id 34%; r.m.s. deviation of 1.3 Å for 259  $\alpha$ -atoms; PDB ID:3RAO) (33), *P. fluorescens* alkanesulfonate

monooxygenase MsuD (seq. id 29%; r.m.s. deviation of 1.4 Å for 255  $\alpha$ -atoms, PDB ID:7JW9) (6), *E. coli* pyrimidine monooxygenase RutA (seq. id 27%; r.m.s. deviation of 1.4 Å for 256

$\alpha$ -atoms, PDB ID:6SGM) (4), and the *Bacillus subtilis* DBT monooxygenase BdsA (seq. id 22%; r.m.s. deviation of 1.8 Å for 242  $\alpha$ -atoms, PDB ID: 5XKC) (36). *SI Appendix, Table S3* shows that the class C monooxygenases have extremely diverse sequence IDs. Their structural integrity is maintained due to the stability of the TIM barrel fold, which can accommodate divergent sequences (37).

**Ligand Binding to SfnG.** The initial analysis of the unliganded structure of SfnG revealed an unbuilt portion of IR-3 (V264–T289) that corresponds to an active site lid region found in class C flavin-dependent monooxygenases (*SI Appendix, Figs. S7 and S8*) (6, 38). Three or four sulfate ions from the crystallization conditions bind along the solvent-exposed active site and tetramer interface, with one of the sulfate ions occupying the expected phosphate binding site from the FMN ribityl moiety (*SI Appendix, Fig. S8 A–E*). A comparison of the liganded and unliganded SfnG structures shows how exposed the active site is without ligands, suggesting conformational changes occur once substrates are bound to close off the active site from bulk solvent (Fig. 4 *A* and *B*). An additional conformational change of the loop following  $\beta$ 5 accompanies FMN binding and results in movement of  $\beta$ 6 and  $\alpha$ 6 of the TIM barrel toward the  $\beta$ 5 strand (*SI Appendix*,

*Fig. S8 F and G*). Despite these changes to the active site, the remainder of the protein shows relatively small differences with an overall r.m.s. deviation of 0.806 Å for 1,043 out of 1,469  $\alpha$  atoms of the tetramer aligned (*SI Appendix, Fig. S8A*). In relation to the tetramer interface, the lid region is directed away from the interface, which would allow active site access for  $\text{FMNH}_2$ ,  $\text{DMSO}_2$ , and  $\text{O}_2$ ; however, a loop of IR-3 makes contacts across the tetramer, which may explain how ligand binding discussed above stabilizes the tetramer interface.

Within the active site of each protomer in the asymmetric unit, there is defined electron density for FMN (Fig. 4*C*). An analysis of FMN binding residues reveals the phosphoryl binding motif including residues H136, Y140, S188, and S189 that are conserved in SfnG (*SI Appendix, Fig. S7*) as well as within class C flavin-dependent monooxygenases. The ribityl moiety is positioned by backbone interactions of G120 and G186 and sidechain interaction with N284 (*SI Appendix, Figs. S8G and S9*). Further analysis of the isoalloxazine ring shows that, in addition to van der Waals interactions, the backbone peptide group of I54 is positioned to engage in two hydrogen-bonding interactions with N3 and an exocyclic C=O of the flavin. Residue W121 in the unliganded structure was extremely disordered in each chain but becomes positioned to interact directly with the isoalloxazine ring

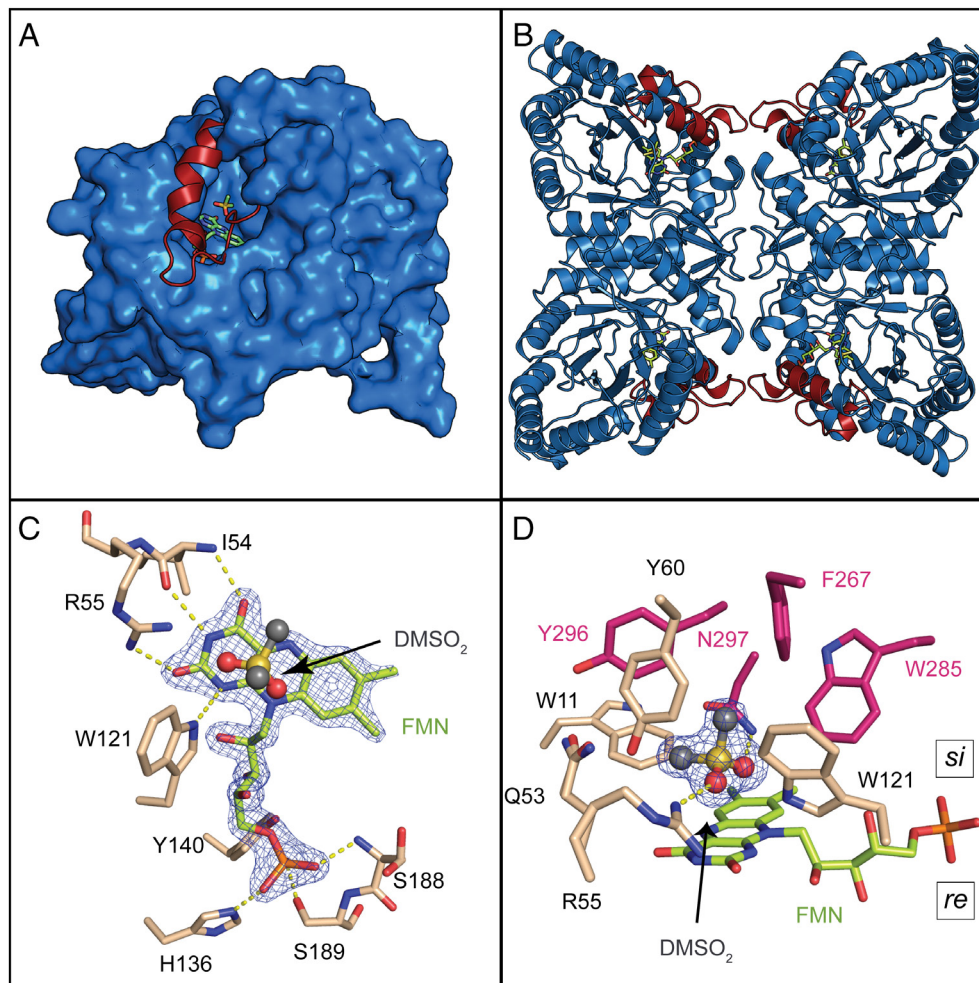


**Fig. 4.** Ligand binding orders the lid region (IR-3) of SfnG and reveals residues involved in substrate binding. (A) A protomer of liganded SfnG is shown in blue surface representation with the ordered lid region of IR-3 displayed in red cartoon. (B) A tetramer of liganded SfnG is shown in blue cartoon representation with the ordered lid region of IR-3 displayed in red cartoon. Atoms are colored as follows: oxygen, red; sulfur, yellow; nitrogen, blue; ligand carbons, green; and phosphorus, orange. SfnG is shown with polder omit maps for (C) FMN and (D)  $\text{DMSO}_2$  contoured at a  $5\sigma$  level. The *si*- and *re*-faces of the FMN isoalloxazine ring are labeled in panel *D*. Carbon atoms of the lid region are colored pink, FMN carbons are green, and  $\text{DMSO}_2$  carbons are dark gray. Hydrogen bonds to FMN and  $\text{DMSO}_2$  are displayed as dashed yellow lines, and hydrogen bonds between protein residues are omitted for clarity.

through hydrogen bonding with N1 (Fig. 4C and *SI Appendix*, Fig. S8E). The last residue to interact with FMN is R55, which positions its guanidino group to interact with an exocyclic C=O of the flavin.

Tetrahedral electron density is observed at the *si*-face of the isoalloxazine ring for DMSO<sub>2</sub>. As crystallization conditions were identified in the presence of the sulfonate buffer MES, we further explored whether MES or a degradation product could be bound within the crystal structure; however, considering that crystals form overnight, we do not expect MES degradation, and neither R-SO<sub>3</sub><sup>1-</sup> nor SO<sub>4</sub><sup>2-</sup> species refine reasonably within the electron density maps (*SI Appendix*, Fig. S10). Several residues were identified that are involved in DMSO<sub>2</sub> binding, all of which are strictly conserved in SfnG enzymes (Fig. 4D and *SI Appendix*, Fig. S7). Residues W121 and R55 are involved in FMN binding and positioned to donate hydrogen bonds to the DMSO<sub>2</sub> oxygen atoms, and residue N297 is positioned to hydrogen bond to the second oxygen of DMSO<sub>2</sub>. The dimethyl groups of DMSO<sub>2</sub> are positioned toward an aromatic cage made up of residues W11 and Y60 of the (β/α)<sub>8</sub> barrel and F267, W285, and Y296 of the lid region within IR-3. Both Y296 and Y60 are positioned to make a second sphere interaction with Q53.

### SfnG Has a Semiconserved O<sub>2</sub> Binding Site for N5 Chemistry that Can Distinguish between Oxygen and Water Binding.

Near the flavin C4a position, Y60 is part of a loop following β2 of the protein core that is observed in two conformations that alter access to the active site, either directed away from (open) or toward (closed) the active site (Fig. 5A). The open and closed loop conformations are only apparent within the ternary complex, the unliganded structure shows the loop positioned away from the active site. Analysis of the Y60 loop in all eight protomers within the asymmetric unit reveals this loop is found on average 35% of the time in the open conformation and 65% of the time in the closed conformation, with flavin and DMSO<sub>2</sub> ligands refining at full occupancy. Refinement of the “closed” structure using phenix ensembler (39), which incorporates limited molecular dynamics simulations into crystallographic refinement, returned a series of models confirming dynamic movement of the Y60 loop (Fig. 5B). Despite the mobility of this loop, however, the *si*-face of the isoalloxazine ring near the C4a is crowded by residues W11, Q53, and R55, in addition to the substrate DMSO<sub>2</sub>, suggesting the oxygen binding site must be elsewhere.

Superimposition of the liganded structure of SfnG with the crystallographic structure of the O<sub>2</sub>-bound RutA homolog (4) identifies a site within SfnG that likely binds O<sub>2</sub> (Fig. 5C). The residues forming the pocket in SfnG consist of L51, I54, A87, I88, N116, V118, and F204, which are positioned similarly to corresponding residues within RutA (4). These residues form a pocket on the *re*-face of the isoalloxazine ring and may direct O<sub>2</sub> toward position N5 of the ring, as is proposed for other members of this family (4). The residue N116 in SfnG most likely plays an important role in retaining the transient polar superoxide species long enough to allow the radical coupling to N5 of the isoalloxazine ring due to its proximity. The substrate and presumed O<sub>2</sub> binding sites are separated on the *si*- and *re*-faces of the flavin, respectively. Oxygen that reacts with FMNH<sup>-</sup> at the *re*-face would require either an inversion of the generated peroxyflavin [as previously proposed for RutA and other related enzymes (4)] or a large conformational change for the monooxygenase reaction to occur. We deem the latter to be unlikely for SfnG given the highly packed active site around the isoalloxazine ring and DMSO<sub>2</sub>. Inversion is forbidden at the C4a position; therefore, SfnG likely proceeds through an N5 oxygenation pathway for generation of

the amino(hydro)peroxide adduct for the oxidative cleavage of DMSO<sub>2</sub>. Indeed, one of the methyl groups of DMSO<sub>2</sub> is positioned 3.9 Å from the flavin N5 position, which is within reasonable distance for oxygenation of the methyl group by an inverted N5-(hydro)peroxyflavin intermediate.

To test whether SfnG employs the N5 of reduced flavin, reactions of SfnG at 150 μM were initiated with substoichiometric FMNH<sup>-</sup> generated within an anaerobic chamber through photoreduction in the presence of EDTA. Using a method previously reported for RutA (40) and CmoJ (9), this reaction mixture of SfnG was incubated with the larger diethyl sulfone and subsequently exposed to oxygen. As the diethylsulfone is larger than DMSO<sub>2</sub>, we reasoned that although some turnover may occur, the SfnG reaction may be perturbed enough to form an N5-oxide by-product (*SI Appendix*, Fig. S11). Separation by LC–MS reveals the formation of a new peak at 473.109 m/z, corresponding to the FMN N5-oxide previously observed in similar experiments for CmoJ and RutA (9, 40), supporting that SfnG utilizes an N5-(hydro)peroxyflavin species. To further probe the putative oxygen binding site, residue N116 was mutated to either alanine or glutamate. Surprisingly, mutation to alanine led to formation of a soluble protein aggregate, whereas the glutamate mutation produced soluble protein capable of being assayed for N5-(hydro)peroxyflavin formation (*SI Appendix*, Fig. S12). Trapping experiments using diethylsulfone with the N116E variant showed a peak at 457.112 m/z, corresponding to oxidized FMN with lack of an FMN N5-oxide peak (*SI Appendix*, Fig. S13).

Further analysis of the structure of SfnG with flavin and DMSO<sub>2</sub> bound reveals an ordered water to be bound in the position where O<sub>2</sub> is expected to bind. Water at this position would donate two hydrogen bonds, thus changing the environment at the *re*-face of the flavin. We observe a geometry consistent with acceptance of a hydrogen bond from N116 and hydrogen bond donation to the N5 flavin position and to the backbone C=O of T52, which exists in two alternate conformations within each protomer of the ternary complex, demonstrating rotation of the backbone amide toward the bound water (Fig. 5D). Due to the positioning of this water in the oxygen binding site, the observed protein backbone conformation would be affected depending on whether water or oxygen/superoxide is present for radical coupling to N5. Next to T52, residue Q53, which is strictly conserved in SfnG sequences (*SI Appendix*, Fig. S7), adopts alternate conformations within the liganded structure. Residues T52 and Q53 connect the oxygen-binding site to the *si*-face of the flavin, where Q53 forms van der Waals contacts with the methyl of DMSO<sub>2</sub> located proximal to the flavin N5 position and hydrogen bonds to the hydroxyphenyl moieties of Y60 and Y296 of the aromatic cage. Therefore, an intermolecular network between the oxygen binding site and the active site lid is observed that can change depending on whether water or oxygen is bound at the *si*-face of the isoalloxazine ring. To disrupt this network of interactions, Q53 was mutated to alanine; however, the Q53A mutant was mainly found within the insoluble protein fraction. Therefore, the soluble Q53E variant was generated and tested using the flavin N5-oxide trapping assay detailed above with diethylsulfone (*SI Appendix*, Figs. S12 and S13). No detectable formation of a flavin N5-oxide peak was observed, which supports the importance of this network of interactions for oxygen reactivity.

**SfnG Can Oxygenate Variable Dialkylsulfones.** SfnG was assayed in the presence of MsuE, NADH, FMN, and either diethyl- or ethylmethylsulfone. Through an endpoint assay analyzed by <sup>1</sup>H NMR spectroscopy, SfnG was shown to convert diethylsulfone to ethanesulfinate and ethylmethylsulfone to both methanesulfinate and ethanesulfinate (Fig. 6A), with presumed concomitant formation

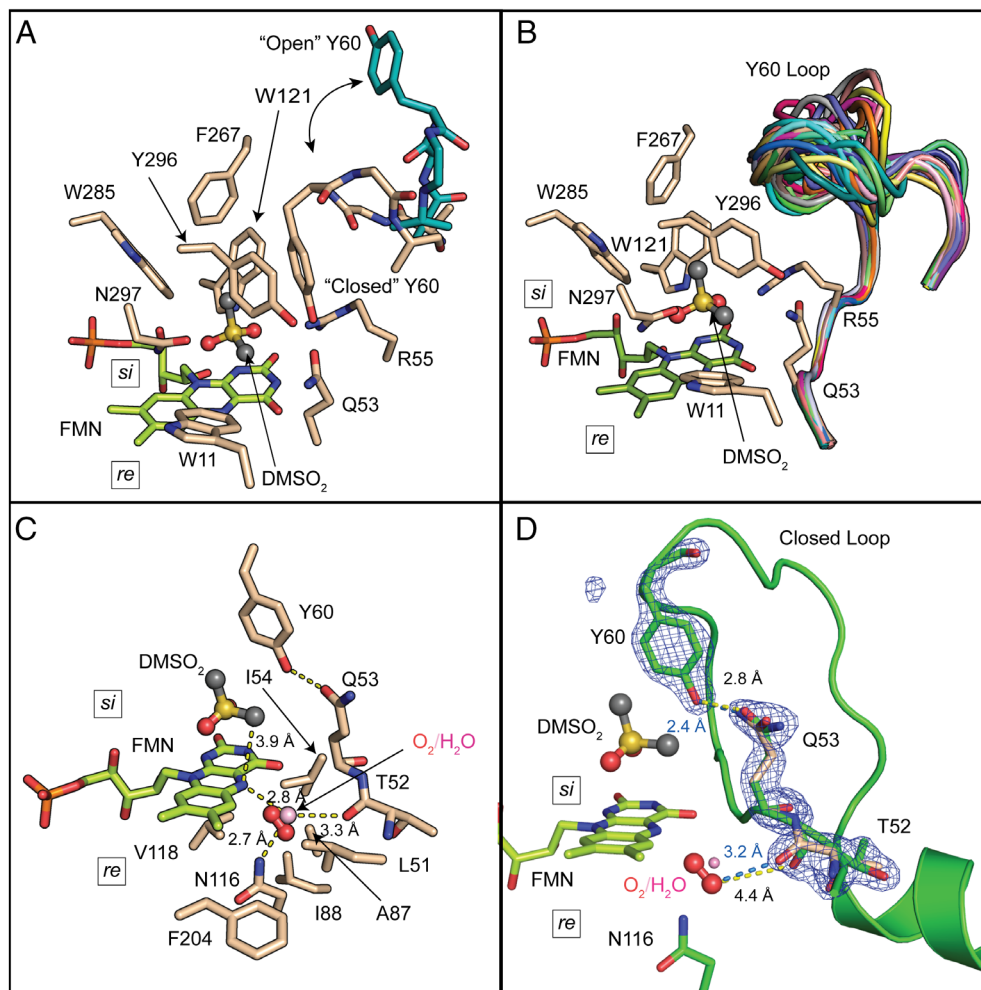


**Fig. 5.** The oxygen binding site and alternate loop conformations reveal a network connecting the substrate/product and oxygen binding sites. (A) A loop containing Y60 (AGYGA) is observed in closed and “open” conformations, colored wheat and teal, respectively. Atoms are colored as in Fig. 4. (B) Ensemble refinement demonstrates flexibility of the AGYGA loop. (C) The dioxygen binding pocket of SfnG is predicted based on homology to RutA (PDB ID 6TEG) (4). In SfnG, an ordered water molecule (pink) overlays with dioxygen (red) from the RutA structure. Hydrogen-bonding distances from the  $\text{H}_2\text{O}$  and the distance of C1 of  $\text{DMSO}_2$  to the flavin-N5 position are shown with dashed yellow lines. (D) Polder omit maps for the two observed conformations of T52, Q53, and Y60 are shown, contoured at a  $5\sigma$  level. The Y60 loop is colored green. Only one of the alternate conformations is displayed in panels A–C for clarity. The *si*- and *re*-faces of the FMN isoalloxazine ring are labeled on each figure.

of acetaldehyde or formaldehyde in both assays. The reaction with ethylmethylsulfone yielded a mixture of the starting substrate with new observed chemical shifts for the products methanesulfinate (*s*,  $\delta$  2.25, 3H) (24) and ethanesulfinate (*q*,  $\delta$  2.30, 2H; *t*  $\delta$  1.05, 3H). The reaction with diethylsulfone yielded a mixture of starting substrate and ethanesulfinate, as well as ethanesulfonate (*q*,  $\delta$  2.87, 2H; *t*  $\delta$  1.24, 3H), presumed from nonenzymatic oxidation of produced ethanesulfinate in the coupled reaction conditions. Therefore, SfnG does not appear to be absolutely specific for  $\text{C}_1$  substrates, but the reaction efficiency is affected, which is consistent with the production of the abortive FMN N5-oxide detailed above.

The observed activity of SfnG with diethyl and ethylmethylsulfone led us to perform docking of diethylsulfone using GLIDE (41). In docking experiments, three poses were obtained that satisfied placement of the two S=O bonds as observed in the ternary crystal structure, positioning  $\text{C}_1$  above the flavin N5 position. Two of these poses positioned the  $\text{C}_2$  carbon toward the N5 position of FMN, which would sterically interfere with the necessary inversion of the N5-(hydro)peroxy species (4) and also would not be consistent with the chemical outcome of the reaction. One pose did position the  $\text{C}_1$  carbon by the flavin N5 position with the  $\text{C}_2$  carbon

rotated away from the flavin, which would enable reaction with the inverted N5-(hydro)peroxy species (Fig. 6*B*). To probe if the observed open Y60 loop conformation facilitated binding of the larger substrates in reactive conformations, docking experiments were performed with Y60 in the “out” conformation. Interestingly, both conformations of Y60 showed the ability to bind diethylsulfone in a manner similar to  $\text{DMSO}_2$ , with an ethyl moiety positioned above the flavin N5 position, but with nonoptimal geometry for catalysis. Therefore, it appears that the active site of SfnG can bind  $\text{C}_2$  species for C–S bond cleavage, but there still needs to be slight movement of the ethyl group for the chemistry to proceed.

## Discussion

FPMOs catalyze a suite of useful bond forming and breaking reactions (1–3) and are separated into distinct classes based on their structure (1). Intriguingly, the identified FPMOs SfnG, MsuD/SsuD, BdsA, and DmoA that catalyze C–S bond cleavage of organosulfur compounds are all class C TC-FMOs, despite sharing <29% sequence identity with each other. SfnG, MsuD, SsuD, and DmoA cleave  $\text{Csp}^3\text{-S}$  bonds whereas BdsA catalyzes the cleavage of DBT sulfone at an  $\text{sp}^2$  hybridized carbon bonded to sulfur. The

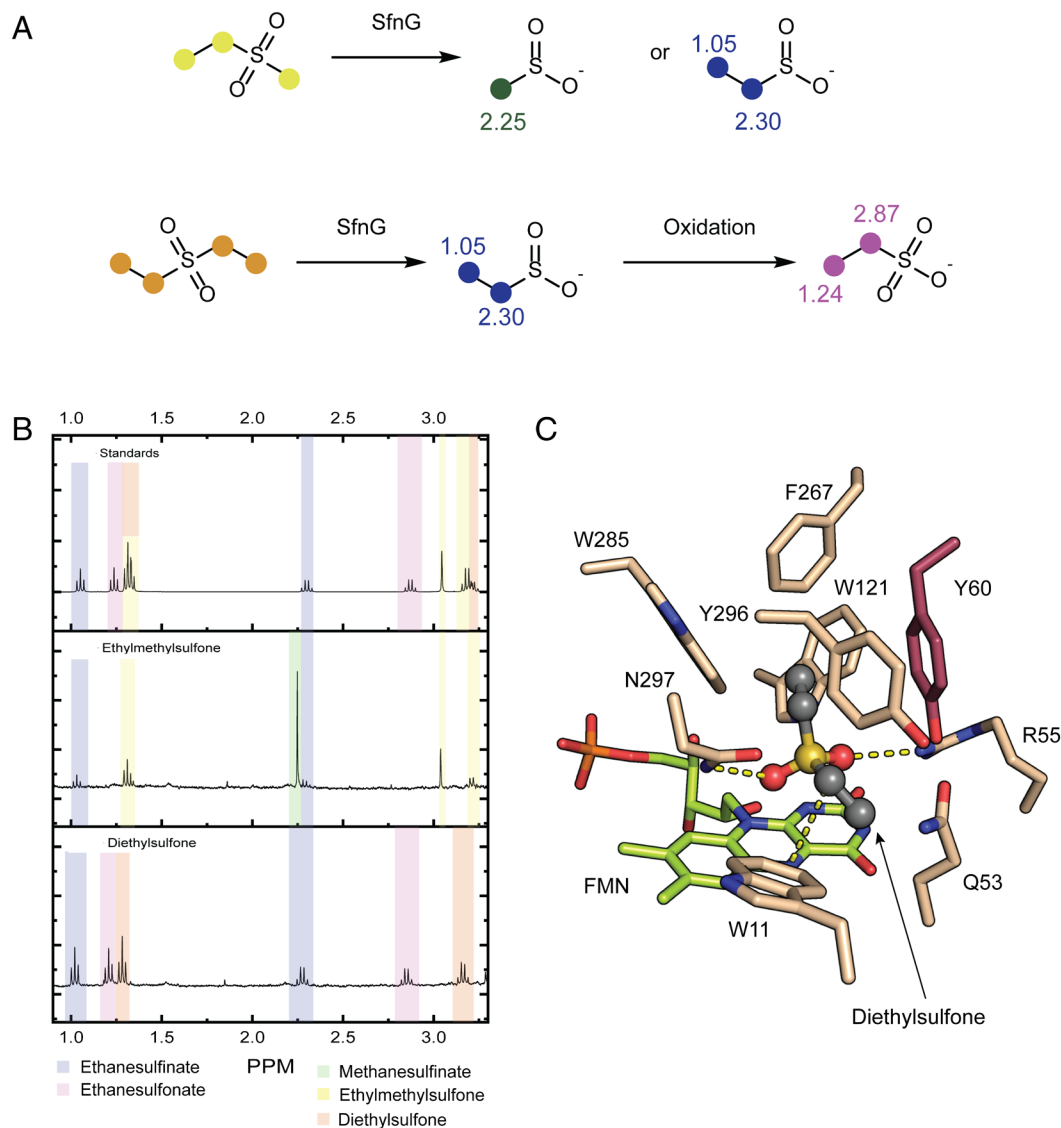


**Fig. 6.** SfnG can accommodate and react with C2 dialkylsulfones. (*A* and *B*) Reactions of SfnG, MsuE, and NADH with either ethylmethylsulfone or diethylsulfone as substrates were monitored using  $^1\text{H}$ -NMR and compared to the NMR resonances of a mixture of authentic samples of the substrates diethylsulfone and ethylmethylsulfone and the possible product ethanesulfonate and its nonenzymatic oxidation product, ethanesulfonate. Molecules are presented and color coded to match corresponding NMR resonances. (*C*) Molecular docking of diethylsulfone (displayed in ball and stick with carbons in dark gray) with SfnG in its closed Tyr60 conformation (carbons in magenta) returns 1 of 10 poses with the sulfone moiety positioned to interact with R55 and N297 and the ethyl moiety directed above the flavin N5-position.

class C TC-FMOs adopt similar homodimeric structures, and MsuD, SsuD, and BdsA form dimer-of-dimer species where helices  $\alpha$ 1 and  $\alpha$ 7 of the  $(\beta/\alpha)_8$  core interact to form a helical bundle with a bulged ring or ellipsoid tetramer structure (*SI Appendix*, Fig. S14) (6, 10, 36, 42). Here, we report that SfnG adds to the possible quaternary states of class C TC-FMOs with the observed butterfly tetramer (6, 10, 42). To verify SfnG behaves as a tetramer in solution, aSEC, SEC-MALS, and DLS were run in low and high salt conditions with and without ligands. Interestingly, the high salt caused a shift from the SfnG tetramer to a dimeric species, whereas binding of FMN or FMN + DMSO<sub>2</sub> stabilized the tetramer.

TC-FMOs require a reductase to provide reduced FMN, and several systems have shown protein–protein interactions exist (43–45). Hydrogen–deuterium exchange assays on the homologous *E. coli* SsuE reductase and SsuD alkanesulfonate monooxygenase system (46) identified surface residues within the active site lid with increased protection from exchange when SsuE is complexed with SsuD, but the location of the active site lid in

SsuD relative to the tetramer interface differs from the tetramer interface observed for SfnG (*SI Appendix*, Fig. S14). How the butterfly quaternary structure of SfnG may affect possible protein–protein interactions with a reductase, many of which form dimers and dimer-of-dimer structures (47), is unknown.

The biophysical characterization of dissociation constants for FMN binding in this system reveals the  $K_D$  for FMN binding to MsuE is an order of magnitude tighter than for the monooxygenases SfnG, MsuC, and MsuD, consistent with FMN serving as a substrate for MsuE and a product for the monooxygenases. In the presence of 1% (v/v) DMSO<sub>2</sub>, the weaker binding in SfnG is primarily due to an increase in the  $k_{off}$  and addition of DMSO<sub>2</sub> further decreases the  $k_{off}$  which would result in tight binding of the flavin in the presence of excess dialkylsulfone substrates. In comparison, the TC-FMO *E. coli* SsuE and SsuD system has  $K_D$  values for FMN binding to SsuE and SsuD of 0.015  $\mu\text{M}$  and 10  $\mu\text{M}$ , respectively (30, 48). This difference between the *E. coli* *ssu* and *P. fluorescens* *sfn* and *msu* systems implies weakened binding of FMN in *P. fluorescens*

MsuE in comparison to *E. coli* SsuE. Similar magnitudes of affinity for FMN have recently been reported for monooxygenases MsuD from *Pseudomonas aeruginosa* (49) and SfnG from *Acinetobacter baumannii* (26).

The active site of class C TC-FMOs is defined by the *re*- and *si*-faces of the isoalloxazine ring of FMN, with the binding of oxygen at a conserved motif buried by the *re*-face (4). The substrate which reacts with the peroxyflavin is bound above the *si*-face, enclosed by a dynamic active site lid region of variable helices (6). In the absence of ligands, the lid region is disordered and the active site and tetramer interface are solvent exposed. Interestingly, both crystallization conditions contained compounds such as MES and  $(\text{NH}_4)_2\text{SO}_4$ ; however, neither MES degradation products such as sulfonates nor sulfates were found to be bound in the active site. The MES molecule itself is too large to fit into the crowded active site. Ethanesulfonate was docked within the active site as a mimic of potential sulfonate degradation products containing an R-SO<sub>3</sub><sup>-</sup> group, but the electron density did not support the presence of a charged oxygen or a longer R chain. In a typical biological environment, SfnG must minimize binding of common cellular polyanions such as phosphate or downstream products of this pathway, such as sulfate or sulfite. The active site of SfnG addresses this challenge by employing an aromatic cage that lacks positively charged residues, which is evolved to bind neutrally charged sulfones. The mobile Y60 loop may play a role in substrate and product release due to its positioning near the surface. However, further investigation is needed to fully understand the role of the mobile Y60 loop.

The observed active site architecture of SfnG is most consistent with formation of an N5-(hydro)peroxyflavin intermediate on the *re*-face of FMN, which can undergo inversion to react with the substrate, DMSO<sub>2</sub>, for SfnG, as proposed for the TC-FMOs RutA, MsuD, SsuD, CmoJ, YxeK, DszA, and HcbA1 (4–9), although the N5-(hydro)peroxyflavin is yet to be observed spectroscopically. Recent stop-flow studies of the *A. baumannii* SfnG with DMSO<sub>2</sub> did not observe formation of a species corresponding to either the N5- or the C4a-(hydro)peroxyflavin (26). Studies of the CmoJ, HcbA1, DszA, and RutA systems have shown the utilization of an N5-oxide as a result of product bond cleavage or through an abortive pathway, which was observed using LC-MS (8, 9, 40, 50). When SfnG from *P. fluorescens* was supplied diethylsulfone, an alternative substrate shown to incompletely react in an NMR endpoint assay, both FMN and the N5-oxide were detected as products by LC-MS. Docking experiments similarly confirmed nonoptimal positioning of diethylsulfone for the reaction. The lack of observed flavin N5-oxide by the N116E variant is consistent with a role for N116 in stabilizing the polar transient superoxide species before radical coupling with the N5 position of the isoalloxazine ring. A glutamate residue at residue 116 would occlude the oxygen binding site and make unfavorable electrostatic interactions with the superoxide species, therefore the N116A variant was also created to prevent occlusion of the oxygen binding site. However, the N116A mutant formed only soluble aggregates, suggesting a polar residue may be necessary within the oxygen binding pocket to stabilize the protein structure.

How the enzyme senses if oxygen is bound has remained an unexplored question. Here, the structure of SfnG shows conformational disorder in the peptide backbone of T52 with a minor conformation directing the backbone carbonyl to hydrogen bond with an observed water molecule bound in the oxygen binding site. This fluctuation would not be favored with dioxygen bound, which could not form favorable interactions with the T52 carbonyl. The adjacent residue, Q53, extends past the isoalloxazine ring to the *si*-face, where it interacts with the

dynamic lid region and the bound DMSO<sub>2</sub>. Mutation of Q53 to alanine caused the protein to become insoluble; however, Q53E was soluble and interestingly showed no measurable flavin N5-oxide species generated when assayed with diethylsulfone. Mutations to Q53 could possibly disrupt dialkylsulfone binding or perturb protein dynamics by altering interactions to Y60 within the dynamic lid region. Overall, T52 and Q53 likely play a role that links the *si*-face to the oxygen binding site found on the *re*-face of FMN. Although RutA (4) similarly contains a longer residue, Met, in the i + 1 position of the residue corresponding to T52 (4), and its amino acid properties match its substrate and active site lid interactions, BdsA, SsuD, and MsuD contain a proline at the i + 1 position. Proline can be involved in hydrophobic packing of substrates of BdsA, SsuD, and MsuD; however, proline also limits the possible backbone torsion angles within the oxygen binding site. Therefore, we predict those TC-FMOs containing a proline at the i + 1 site would have a more rigid oxygen binding site. How increased rigidity affects oxygen binding and/or release of reactive oxygen intermediates remains to be seen, and future studies of the structural fluctuations identified here will inform upon features of the oxygen binding site for catalysis and protection of the putative reactive N5-(hydro)peroxyflavin intermediate.

Currently, there are two proposed mechanisms for C–S bond cleavage at *sp*<sup>3</sup> carbon centers via a N5-(hydro)peroxyflavin intermediate from work studying YxeK (5) and MsuD (6). Both mechanisms share the same activation of molecular oxygen to react with reduced FMN, yielding the N5-peroxyflavin (*SI Appendix*, Fig. S15 A, B). Invoking the S<sub>N</sub>2 proposal for SfnG (*SI Appendix*, Fig. S15A), direct nucleophilic attack by the N5-peroxyflavin would release methanesulfinate with an alkylated N5-peroxyflavin, which resolves to form FMN, formaldehyde, and water (5). The alternative mechanistic proposal (*SI Appendix*, Fig. S14B) would involve hydroxylation at the C1 position (6), which breaks down to form formaldehyde and methanesulfinate with generation of FMN and water. Most recently, Mangkalee et al. propose that SfnG may directly produce peroxide to react with DMSO<sub>2</sub> within the active site (26), but diffusion of peroxide from the putative oxygen binding site to react with bound DMSO<sub>2</sub> appears less favorable than a covalent intermediate species. Nonetheless, an NMR endpoint assay was used to determine whether SfnG was specific for DMSO<sub>2</sub>, and the data show that SfnG could cleave both diethylsulfone and mixed ethylmethylsulfone at the C1 position of methyl and ethyl-subunits, indicating SfnG can accommodate either group's C1 near the flavin N5 position. The C1 position of ethyl-containing sulfones was found to dock in a state that is not optimal for either S<sub>N</sub>2 attack or hydroxylation, suggesting additional movements may be needed for reactivity, which may be amenable from the dynamic active site lid region. Future studies will be needed to explore the mechanistic possibilities.

In summary, we have presented biophysical characterization of FMN binding within the DMSO<sub>2</sub> utilization system from *P. fluorescens* and crystal structures of the TC-FMO SfnG, which catalyzes the first C–S bond cleavage within sulfur assimilation from DMSO<sub>2</sub>. The 1.75-Å resolution structure with FMN and DMSO<sub>2</sub> bound reveals the molecular details for placement of ligands within an ordered enzyme active site and lid region, but with alternate conformations of residues in the oxygen binding pocket and a mobile Y60 loop. Flavin N5-oxide trapping experiments and the placement of ligands and the predicted oxygen-binding site on opposite faces of the flavin are most consistent with the C–S cleavage occurring through an N5-(hydro)peroxyflavin pathway. These results reveal a butterfly tetramer architecture previously unobserved within class C TC-FMOs and provide high-resolution

information toward understanding C–S bond-cleavage, representing possible areas of future exploration in bioengineering of FPMOs, as well as of antibiotic development against pathogenic *Pseudomonads* dependent on sulfur assimilation for pathogenesis.

## Materials and Methods

Recombinant protein samples for *P. fluorescens* MsuC, MsuD, MsuE, and SfnG (*SI Appendix, Fig. S16*), and generated SfnG variants, were expressed and purified as detailed in *SI Appendix, Supporting Methods*, based on previously reported methods (6, 24, 27). Multiangle and dynamic light scattering were performed on the Dawn Ambient and NanoStar II systems (Waters-Wyatt Technologies) and SPR spectroscopy experiments were performed using a Cytiva biacore 8k system, with details in *SI Appendix, Supporting Methods*. Fluorescence titration FMN binding studies were performed on a Jasco FP-8350 using previously reported methods (51) and adapted as detailed in *SI Appendix, Supporting Methods*. Trapping assays of the flavin N5-oxide and measurement by LC-MS are based on previous reports (9, 40) and detailed in *SI Appendix, Supporting Methods*. Crystallography of purified SfnG, X-ray diffraction experiments, model building, refinements, and molecular docking of diethylsulfone are detailed in *SI Appendix, Supporting Methods*. Endpoint activity assays with alternative dialkylsulfones were performed as in ref. 24 with modifications as detailed in *SI Appendix, Supporting Methods*.

**Data, Materials, and Software Availability.** The atomic coordinates and structure factors have been deposited in the Protein Data Bank, [www.pdb.org](http://www.pdb.org) [PDB ID codes 8TOU (unliganded) (52) and 8TOW (liganded) (53)]. All other data are included in the manuscript and/or *SI Appendix*.

**ACKNOWLEDGMENTS.** We kindly acknowledge Robert Grant and the Massachusetts Institute of Technology Structural Biology Core facility, as well as the Northeastern Collaborative Access Team beamlines, funded by the National Institute of General Medical Sciences from the NIH (P30 GM124165), within the Advanced Photon Source, a U.S. Department of Energy (DOE) Office of Science User Facility operated for the DOE Office of Science by Argonne National Laboratory under Contract No. DE-AC02-06CH11357. We acknowledge the Biophysical Instrumentation Core and the Proteomics Core at the University of Massachusetts Boston, funded by the Massachusetts Life Sciences Center. We thank Karen Allen and James Conley for aid in collecting initial dynamic light scattering data. We thank Holly Ellis, Shruti Somai, and Chioma Helen Aloh for thoughtful discussions. This work was supported by the NSF, USA [1807480 to D.K.W. and D.P.D., and 2105998 subaward to D.P.D.]. Opinions, findings, and conclusions or recommendations expressed are those of the authors and do not necessarily reflect the views of the NSF.

Author affiliations: <sup>a</sup>Department of Chemistry, University of Massachusetts, Boston, MA 02125; and <sup>b</sup>Department of Biochemistry, Chemistry, Environment, and Physics, Suffolk University, Boston, MA 02108

- C. E. Paul, D. Eggerichs, A. H. Westphal, D. Tischler, W. J. H. van Berkel, Flavoprotein monooxygenases: Versatile biocatalysts. *Biotechnol. Adv.* **51**, 107712 (2021).
- M. Toplak, R. Teufel, Three rings to rule them all: How versatile flavoenzymes orchestrate the structural diversification of natural products. *Biochemistry* **61**, 47–56 (2022).
- E. Romero, J. R. Gomez Castellanos, G. Gadda, M. W. Fraaije, A. Mattevi, Same substrate, many reactions: Oxygen activation in flavoenzymes. *Chem. Rev.* **118**, 1742–1769 (2018).
- A. Matthews *et al.*, Aminoperoxide adducts expand the catalytic repertoire of flavin monooxygenases. *Nat. Chem. Biol.* **16**, 556–563 (2020).
- A. Matthews *et al.*, Bacterial flavoprotein monooxygenase YxeK salvages toxic S-(2-succino)-adducts via oxygenolytic C-S bond cleavage. *FEBS J.* **289**, 787–807 (2022).
- J. J. M. Liew, I. El Saudi, S. V. Nguyen, D. K. Wicht, D. P. Dowling, Structures of the alkanesulfonate monooxygenase MsuD provide insight into C–S bond cleavage, substrate scope, and an unexpected role for the tetramer. *J. Biol. Chem.* **297**, 100823 (2021). 10.1016/j.jbc.2021.100823.
- Y. Guo, D. F. Li, H. Ji, J. Zheng, N. Y. Zhou, Hexachlorobenzene monooxygenase substrate selectivity and catalysis: Structural and biochemical insights. *Appl. Environ. Microbiol.* **87**, e01965–e01920 (2020).
- S. Adak, T. P. Begley, Dibenzothiophene catabolism proceeds via a flavin-N5-oxide intermediate. *J. Am. Chem. Soc.* **138**, 6424–6426 (2016).
- S. Hazra, T. P. Begley, Alkylcysteine sulfoxide C–S monooxygenase uses a flavin-dependent Pummerer rearrangement. *J. Am. Chem. Soc.* **145**, 11933–11938 (2023).
- E. Eichhorn, C. A. Davey, D. F. Sargent, T. J. Richmond, Crystal structure of *Escherichia coli* alkanesulfonate monooxygenase SsuD. *J. Mol. Biol.* **324**, 457–468 (2002).
- R. Bentley, T. G. Chasten, Environmental VOCs—Formation and degradation of dimethyl sulfide, methanethiol and related materials. *Chemosphere* **55**, 291–317 (2004).
- M. Giardano, A. Norici, R. Hell, Sulfur and phytoplankton: Acquisition, metabolism and impact on the environment. *New Phytol.* **166**, 371–382 (2005).
- A. Edtbauer *et al.*, A new marine biogenic emission: Methane sulfonamide (MSAM), dimethyl sulfide (DMS), and dimethyl sulfone (DMSO<sub>2</sub>) measured in air over the Arabian Sea. *Atmos. Chem. Phys.* **20**, 6081–6094 (2020).
- R. Boden, L. P. Hutt, “Bacterial metabolism of C1 sulfur compounds” in *Aerobic Utilization of Hydrocarbons, Oils and Lipids, Handbook of Hydrocarbon and Lipid Microbiology*, F. Rojo, Ed. (Springer Nature, Switzerland AG, 2019), pp. 1–43.
- A. M. Traynor, K. J. Sheridan, G. W. Jones, J. A. Calera, S. Doyle, Involvement of sulfur in the biosynthesis of essential metabolites in pathogenic fungi of animals, particularly *Aspergillus* spp.: Molecular and therapeutic implications. *Front. Microbiol.* **10**, 2859 (2019).
- X. He, C. M. Slupsky, Metabolic fingerprint of dimethyl sulfone (DMSO<sub>2</sub>) in microbial-mammalian co-metabolism. *J. Proteome Res.* **13**, 5281–5292 (2014).
- T. L. Poole, R. Benjamin, K. J. Genovese, D. J. Nisbet, Methylsulfonylmethane exhibits bacteriostatic inhibition of *Escherichia coli*, and *Salmonella enterica* Kinshasa, *in vitro*. *J. Appl. Microbiol.* **127**, 1677–1685 (2019).
- M. A. Kertesz, Riding the sulfur cycle—Metabolism of sulfonates and sulfate esters in Gram-negative bacteria. *FEMS Microbiol. Rev.* **24**, 135–175 (1999).
- D. P. Kelly, N. A. Smith, “Organic sulfur compounds in the environment. Biogeochemistry, microbiology, and ecological aspects” in *Advances in Microbial Ecology*, K. C. Marshall, Ed. (Plenum Press, New York, NY, 1990), vol. **11**, pp. 345–385.
- A. R. Autry, J. W. Fitzgerald, Sulfonate S: A major form of forest soil organic sulfur. *Biol. Fertil. Soils* **10**, 50–56 (1990).
- E. Eichhorn, J. R. van der Ploeg, T. Leisinger, Characterization of a two-component alkanesulfonate monooxygenase from *Escherichia coli*. *J. Biol. Chem.* **274**, 26639–26646 (1999).
- E. Eichhorn, J. R. van der Ploeg, M. A. Kertesz, T. Leisinger, Characterization of an  $\alpha$ -ketoglutarate-dependent taurine dioxygenase from *Escherichia coli*. *J. Biol. Chem.* **272**, 23031–23036 (1997).
- M. A. Kertesz, K. Schmidt-Larbig, T. Wuest, A novel reduced flavin mononucleotide-dependent methanesulfonate sulfonatase encoded by the sulfur-regulated msu operon of *Pseudomonas aeruginosa*. *J. Bacteriol.* **181**, 1464–1473 (1999).
- D. K. Wicht, The reduced flavin-dependent monooxygenase SfnG converts dimethylsulfone to methanesulfinate. *Arch. Biochem. Biophys.* **604**, 159–166 (2016).
- B. F. Lei, S. C. Tu, Gene overexpression, purification, and identification of a desulfurization enzyme from *Rhodococcus* sp. strain IGT8 as a sulfide/sulfoxide monooxygenase. *J. Bacteriol.* **178**, 5699–5705 (1996).
- M. Mangkale *et al.*, Reaction mechanism and kinetics of the two-component flavoprotein dimethyl sulfone monooxygenase system: Using hydrogen peroxide for monooxygeination and substrate cleavage. *FEBS J.* **290**, 5171–5195 (2023). 10.1111/febs.16916.
- J. Soule *et al.*, Structure and function of the two-component flavin-dependent methanesulfonate monooxygenase within bacterial sulfur assimilation. *Biochem. Biophys. Res. Commun.* **522**, 107–112 (2020).
- H. R. Ellis, The FMN-dependent two-component monooxygenase systems. *Arch. Biochem. Biophys.* **497**, 1–12 (2010).
- M. Fischer, A. P. Leech, R. E. Hubbard, Comparative assessment of different histidine-tags for immobilization of protein onto surface plasmon resonance sensorchips. *Anal. Chem.* **83**, 1800–1807 (2011).
- X. Zhan, R. A. Carpenter, H. R. Ellis, Catalytic importance of the substrate binding order for the FMNH<sub>2</sub>-dependent alkanesulfonate monooxygenase enzyme. *Biochemistry* **47**, 2221–2230 (2008).
- M. Mangkale *et al.*, Reaction mechanism and kinetics of the two-component flavoprotein dimethyl sulfone monooxygenase system: Using hydrogen peroxide for monooxygeination and substrate cleavage. *FEBS J.* **290**, 5171–5195 (2023).
- T. Endoh, H. Habe, H. Nojiri, H. Yamane, T. Omori, The  $\sigma^{54}$ -dependent transcriptional activator SfnR regulates the expression of the *Pseudomonas putida* sfnG operon responsible for dimethyl sulphone utilization. *Mol. Microbiol.* **55**, 897–911 (2005).
- M. J. Domagalski *et al.*, Crystal structure of the luciferase-like monooxygenase from *Bacillus cereus* ATCC 10987. *PDB*. <https://doi.org/10.2210/pdb3RAO/pdb>. Deposited 28 March 2011.
- D. W. Banner *et al.*, Structure of chicken muscle triose phosphate isomerase determined crystallographically at 2.5 Å resolution using amino acid sequence data. *Nature* **255**, 609–614 (1975).
- E. Krissinel, K. Henrick, Inference of macromolecular assemblies from crystalline state. *J. Mol. Biol.* **372**, 774–797 (2007).
- T. Su *et al.*, Structural and biochemical characterization of BdsA from *Bacillus subtilis* WU-S2B, a key enzyme in the “4S” desulfurization pathway. *Front. Microbiol.* **9**, 231 (2018).
- M. S. Vijayabaskar, S. Vishweshwara, Insights into the fold organization of TIM barrel from interaction energy based structure networks. *PLoS Comput. Biol.* **8**, e1002505 (2012).
- S. Y. Jun, K. M. Lewis, B. Youn, L. Xun, C. Kang, Structural and biochemical characterization of EDTA monooxygenase and its physical interaction with a partner flavin reductase. *Mol. Microbiol.* **100**, 989–1003 (2016).
- B. T. Burnley, P. V. Afonine, P. D. Adams, P. Gros, Modelling dynamics in protein crystal structures by ensemble refinement. *eLife* **1**, e00311 (2012).
- S. Adak, T. P. Begley, RutA-catalyzed oxidative cleavage of the uracil amide involves formation of a flavin-N5-oxide. *Biochemistry* **56**, 3708–3709 (2017).
- R. A. Friesner *et al.*, Extra precision slide: Docking and scoring incorporating a model of hydrophobic enclosure for protein–ligand complexes. *J. Med. Chem.* **49**, 6177–6196 (2006).
- M. Okai *et al.*, Crystal structure of dibenzothiophene sulfone monooxygenase BdsA from *Bacillus subtilis* WU-S2B. *Proteins* **85**, 1171–1177 (2017).
- K. Abdurachim, H. R. Ellis, Detection of protein–protein interactions in the alkanesulfonate monooxygenase system from *Escherichia coli*. *J. Bacteriol.* **188**, 8153–8159 (2006).

44. H. Li *et al.*, Biochemical characterization of the two-component flavin-dependent monooxygenase involved in vananimycin biosynthesis. *Biochemistry* **60**, 31–40 (2021).
45. J. Sucharitakul, R. Tinikul, P. Chaiyen, Mechanisms of reduced flavin transfer in the two-component flavin-dependent monooxygenases. *Arch. Biochem. Biophys.* **555–556**, 33–46 (2014).
46. P. V. Dayal, H. Singh, L. S. Busenlehner, H. R. Ellis, Exposing the alkanesulfonate monooxygenase protein–protein interaction sites. *Biochemistry* **54**, 7531–7538 (2015).
47. C. H. Aloh, T. N. Zeczycki, H. R. Ellis, Oligomeric changes regulate flavin transfer in two-component FMN reductases involved in sulfur metabolism. *Biochemistry* **62**, 2751–2762 (2023).
48. B. Gao, H. R. Ellis, Altered mechanism of the alkanesulfonate FMN reductase with the monooxygenase enzyme. *Biochem. Biophys. Res. Commun.* **331**, 1137–1145 (2005).
49. S. Somai, K. Yue, O. Acevedo, H. R. Ellis, Shorter alkanesulfonate carbon chains destabilize the active site architecture of SsuD for desulfonation. *Biochemistry* **62**, 85–94 (2023).
50. S. Adak, T. P. Begley, Hexachlorobenzene catabolism involves a nucleophilic aromatic substitution and flavin-N5-oxide formation. *Biochemistry* **58**, 1181–1183 (2019).
51. J. M. Robbins, H. R. Ellis, Investigations of two-component flavin-dependent monooxygenase systems. *Methods Enzymol.* **620**, 399–422 (2019).
52. R. Gonzalez, J. Soule, D. P. Dowling, Crystal structure of dimethylsulfone monooxygenase SfNG from *Pseudomonas fluorescens*. RCSB Protein Data Bank. <http://www.rcsb.org/structure/8TOU>. Deposited 1 June 2023.
53. R. Gonzalez, J. Soule, D. P. Dowling, Crystal structure of dimethylsulfone ( $\text{DMSO}_2$ ) monooxygenase SfNG from *Pseudomonas fluorescens* with  $\text{DMSO}_2$  and oxidized FMN bound. RCSB Protein Data Bank. <http://www.rcsb.org/structure/8TOW>. Deposited 1 June 2023.